JOURNAL OF SPACECRAFT AND ROCKETS
Vol. 39, No. 3, May–June 2002

Linearized Motion of a Fin-Stabilized Projectile Subjected to a Lateral Impulse

Bernard J. Guidos* and Gene R. Cooper†
U.S. Army Research Laboratory, Aberdeen Proving Ground, Maryland 21005-5066

An existing analytical theory for modeling the free-flight motion of nonspinning, statically stable projectiles is extended to include the effect of a simple lateral impulse applied during flight. The extended theory is based on the incorporation of generalized lateral translational and angular disturbances into the familiar equations of projectile free-flight motion. The applied disturbances are then modeled using specified mathematical forms, and the modified equations are solved to obtain the angular and translational motion of the projectile over the trajectory. The various components of the translational motion of the projectile are extracted and characterized. An idealized application is presented for a large-caliber finned projectile, representative of the class of 120-mm-long rod finned projectiles fired from current tracked vehicle weapon systems, subjected to a single lateral control impulse in flight. The closed-form analytical solutions are compared against results obtained using a numerical trajectory simulation code that incorporates generalized guidance and control commands.

Nomenclature

A = reference area, $\pi d^2/4$, m^2
$C_{L\alpha}$ = derivative of aerodynamic lift force coefficient with respect to angle of attack
$C_{M\alpha}$ = derivative of aerodynamic pitching moment coefficient with respect to angle of attack
$\tilde{C}_{M1}$ = complex normalized applied moment coefficient
$\tilde{C}_{N1}$ = complex normalized applied lateral force coefficient
d = reference diameter, m
d_F = distance from c.g. to location of applied force, negative if applied aft of c.g., m
$\boldsymbol{F}_1$ = applied translational disturbance vector, N
$\tilde{F}_1$ = complex applied translational disturbance, N
$\tilde{\mathcal{F}}_1^*$ = complex normalized applied translational impulse
g = gravitational constant, m/s^2
h = Heaviside unit step function
$\boldsymbol{I}, \boldsymbol{J}, \boldsymbol{K}$ = Earth-fixed Cartesian coordinate system unit vectors
I_t = transverse moment of inertia, kg · m^2
$\boldsymbol{i}, \boldsymbol{j}, \boldsymbol{k}$ = nonrolling coordinate system unit vectors aligned with projectile velocity vector
$\tilde{\mathcal{J}}_1^*$ = complex normalized applied angular impulse quantity, $\tilde{\mathcal{M}}_1^*/k_t^2$
$K_{j,n}$ = magnitude of jth complex modal arm in nth interval, rad
$\tilde{K}_{j,n}$ = jth complex reference modal arm in nth interval, rad
k_t = normalized radius of gyration, caliber
$\boldsymbol{M}_1$ = applied angular disturbance vector, N · m
$\tilde{M}_1$ = complex applied angular disturbance, N · m
$\tilde{\mathcal{M}}_1^*$ = complex normalized applied angular impulse
m = projectile mass, kg
$\tilde{r}$ = complex lateral displacement, caliber
$\tilde{r}_A$ = nonfluctuating complex lateral displacement attributable to aerodynamic effects, caliber
$\tilde{r}_L$ = complex lateral displacement attributable to all aerodynamic effects, caliber
$\tilde{r}_T$ = complex lateral displacement attributable to translational component of applied disturbance, caliber
s = distance along flight path, caliber
t = time, s
V = magnitude of projectile velocity vector, m/s
$\boldsymbol{V}$ = projectile velocity vector, m/s
X, Y, Z = Earth-fixed coordinates, m
x, y, z = Earth-fixed coordinates normalized by projectile reference diameter, caliber
$\boldsymbol{x}, \boldsymbol{y}, \boldsymbol{z}$ = rolling body-fixed coordinate system unit vectors, m
α = pitch angle
β = yaw angle
δ = Dirac delta function
$\tilde{\theta}$ = complex angular deviation relative to gun muzzle
$\tilde{\theta}_A$ = nonfluctuating complex angular deviation attributable to aerodynamic effects
$\tilde{\theta}_T$ = complex angular deviation attributable to translational component of applied disturbance
$\tilde{\xi}$ = complex angle of attack, $\alpha + i\beta$
$\phi_{j,n}$ = jth reference phase angle in nth interval
$\phi'_{j,n}$ = jth reference phase angle turning rate in nth interval
ϕ_n = orientation of nth applied translational impulse

Superscripts

q' = derivative of quantity q with respect to s
q^* = normalization of quantity q by density factor, $\rho Ad/(2m)$

Introduction

MANY engineering problems in exterior ballistics require an understanding of applied lateral disturbances and their effect on projectile motion. An important example is the guidance and control of munitions, in which lateral course correction maneuvers are applied to alter the trajectory of the flight body. Other examples include yaw card impacts in small arms projectile testing,[1,2] sabot discard disturbances of tank-launched long-rod finned projectiles,[3] close proximity explosions meant to deflect projectiles,[4] and impingement of helicopter rotor downwash on tube-launched rockets.[5]

Linearized motion of projectiles has long formed a basis for aerodynamics testing and analysis, addressing a projectile's continuous free-flight motion occurring in a single interval.[6–10] However, the application of an impulsive lateral disturbance to a projectile in free flight produces additional intervals of continuous motion to be modeled, each having its own flight dynamics parameters. The generalization of single-interval linearized theory to include lateral

Presented as Paper 2000-0767 at the 38th Aerospace Sciences Meeting, Reno, NV, 10–13 January 2000; received 22 August 2000; revision received 24 September 2001; accepted for publication 5 October 2001.

*Aerospace Engineer, Aerodynamics Branch. Senior Member AIAA.
†Research Physicist, Aerodynamics Branch.

impulsive disturbances and multiple intervals is a useful approach for modeling the flight dynamics of such problems. Linearized projectile translational and angular motion can be modeled using generalized mathematical functions to represent the applied disturbances. By incorporating these functions into the existing single-interval linearized equations of free-flight motion, closed-form analytical expressions are produced that show straightforward relationships to exist between the applied impulsive disturbances and the projectile motion.

In the present work, two specific classes of generalized mathematical functions are incorporated into a simplified set of linearized equations of motion for symmetric, nonspinning, statically stable, projectiles. The resulting closed-form expressions have the potential to reduce the computational overhead associated with projectile motion control. The procedure also leads to a generalized framework useful for analyzing observed projectile motion or designing complex guidance and control maneuvers. An application is presented for an idealized large-caliber finned projectile subjected to a single, simple in-flight lateral impulsive disturbance. The modeled motion is compared to that obtained using a six-degree-of-freedom numerical trajetory simulation code that has a guidance and control capability.[11]

Applied Force and Moment Disturbances

The coordinate systems of McCoy[10] are adopted here and are illustrated in Fig. 1. The $(\boldsymbol{I}, \boldsymbol{J}, \boldsymbol{K})$ system is the Earth-fixed range system, the $(\boldsymbol{i}, \boldsymbol{j}, \boldsymbol{k})$ system is a nonrolling system aligned with the velocity vector, and the $(\boldsymbol{x}, \boldsymbol{y}, \boldsymbol{z})$ system is a body-fixed system. When only flat-fire trajectories are considered, the unit vector $\boldsymbol{j}$ is usually aligned to within 1 deg or less with the unit vector $\boldsymbol{J}$, and the unit vector $\boldsymbol{k}$ is usually aligned even closer with the unit vector $\boldsymbol{K}$.

The projectile, in free-flight, is acted on by a lateral impulsive disturbance. The disturbance can be separated into a translational component, that is, a force, $\boldsymbol{F}$ and an angular component, that is, a moment, $\boldsymbol{M}$, both defined as functions of time. In range coordinates and vector form they are

$$\boldsymbol{F} = \boldsymbol{F}(t) = F_Y \boldsymbol{J} + F_Z \boldsymbol{K} \tag{1}$$

$$\boldsymbol{M} = \boldsymbol{M}(t) = M_Y \boldsymbol{J} + M_Z \boldsymbol{K} \tag{2}$$

in which the usual right-hand rule applies to the moment components.

The forms of the lateral disturbances $\boldsymbol{F}$ and $\boldsymbol{M}$ are completely general in actual projectile flight. The approach introduced here specifies simple modeled forms of the disturbances that can be extended and used in more advanced applications to model actual, more generalized, disturbances. Two basic mathematical forms of applied impulsive disturbances are of interest here. The first is referred to here as a finite pulse disturbance, defined as a finite duration, constant amplitude, unidirectional disturbance, having the form

$$\boldsymbol{F}_1 = F_1[\cos\phi_1 \boldsymbol{J} + \sin\phi_1 \boldsymbol{K}] \tag{3}$$

in which the subscript 1 denotes one of any number of disturbances that could be modeled. The orientation of the applied lateral

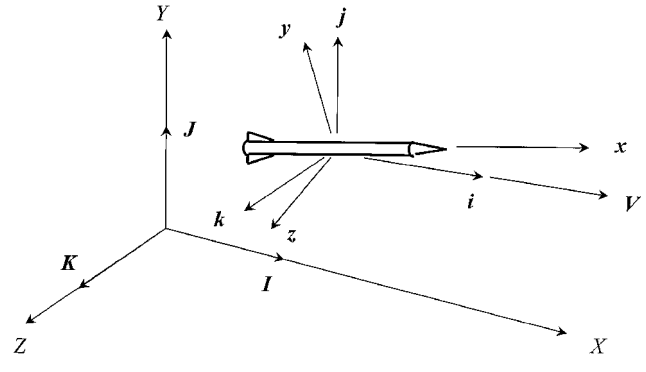

Fig. 1 Coordinate systems.

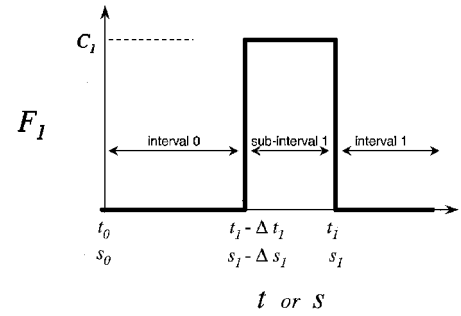

Fig. 2 Finite pulse disturbance.

disturbance about the X axis is ϕ_1 and is constant, and the magnitude is F_1 with the restriction

$$F_1 = F_1(t) = C_1[h(t - t_1 + \Delta t_1) - h(t - t_1)] \tag{4}$$

for $t_1 - \Delta t_1 < t < t_1$, in which C_1 is a real constant and $h(t - t_1)$ is the Heaviside unit step function occurring at t_1, as defined by Lighthill.[12] The form of F_1 is illustrated in Fig. 2. This form of applied disturbance is referred to here as a finite pulse disturbance. The disturbance creates two intervals and one subinterval, also illustrated in Fig. 2, with which motion parameters will eventually be associated. Concurrently, the disturbance can be described in terms of distance along the flight path s as illustrated.

The second form of disturbance considered here one of infinitesimal duration, referred to here as a singular disturbance. A specific form of the finite pulse disturbance, the singular disturbance, is defined here in the same manner as the finite pulse disturbance but with the additional restrictions that $\Delta t_1 \to 0$ (or, concurrently, $\Delta s_1 \to 0$), whereas the modeled impulse remains constant. The singular disturbance is an important form for representing actual disturbances because it is mathematically simple and because it forms a building block with which to model more complicated impulses and motions. The term singular as used here refers to the disturbance's infinitesimal duration and is not intended to denote the presence of a mathematical singularity that does not, in fact, exist in the modeled problem.

The modeled force and moment disturbances are to be incorporated into the free-flight equations of motion that are presented and solved by Murphy[9] and McCoy.[10] The ensuing development requires that the applied lateral force and moment disturbances be cast in complex notation and that the following complex representations are defined consistent with McCoy[10]:

$$\tilde{F}_1 = F_Y + iF_Z \tag{5}$$

$$\tilde{M}_1 = M_Z - iM_Y \tag{6}$$

in which i is the square root of -1. The applied disturbances are normalized to form complex force and moment coefficients $\tilde{C}_{N1}$ and $\tilde{C}_{M1}$, respectively:

$$\tilde{C}_{N1} = \tilde{C}_{N1}(t) = \tilde{F}_1 \Big/ \left(\tfrac{1}{2}\rho V^2 A\right) \tag{7}$$

$$\tilde{C}_{M1} = \tilde{C}_{M1}(t) = \tilde{M}_1 \Big/ \left(\tfrac{1}{2}\rho V^2 Ad\right) \tag{8}$$

The ensuing development also requires the formation of starred quantities, obtained by multiplying the original quantity with the density factor, that is,

$$\tilde{C}^*_{N1} = [\rho Ad/(2m)]\tilde{C}_{N1} \tag{9}$$

$$\tilde{C}^*_{M1} = [\rho Ad/(2m)]\tilde{C}_{M1} \tag{10}$$

The corresponding translational and angular impulses are $\tilde{\mathcal{F}}^*_1$ and $\tilde{\mathcal{M}}^*_1$, respectively. They are complex constants found by integrating the applied disturbances over their duration, that is,

$$\tilde{\mathcal{F}}_1^* = \int_{s_1 - \Delta s_1}^{s_1} \tilde{C}_{N1}^* \, \mathrm{d}s \tag{11}$$

$$\tilde{\mathcal{M}}_1^* = \int_{s_1 - \Delta s_1}^{s_1} \tilde{C}_{M1}^* \, \mathrm{d}s \tag{12}$$

The integrations are performed with respect to flight path s. The disturbances begin at $s_1 - \Delta s_1$, end at s_1, and have a spatial duration of Δs_1. The appropriate transformation of the limits of integration from time t to distance along the flight path s is applied.

The vertical and horizontal components of the translational impulse $\mathcal{F}_Z^*$ and $\mathcal{F}_Y^*$, respectively, are defined in complex notation from

$$\tilde{\mathcal{F}}_1^* = \mathcal{F}_Y^* + i\mathcal{F}_Z^* \tag{13}$$

The translational impulse can be written in polar form as

$$\tilde{\mathcal{F}}_1^* = \mathcal{F}_1^* \exp(i\phi_1) \tag{14}$$

in which the magnitude is $\mathcal{F}_1^*$ and the orientation is ϕ_1. With the coordinate system definitions as presented thus far, $\phi_1 = 0$ deg corresponds to a translational impulse oriented in the positive $\boldsymbol{Y}$ direction, or upward.

The applied force vector associated with, for example, a lateral pulse generator, is typically coplanar with and perpendicular to the projectile axis. If the pitch and yaw angles are small, then the components of the force vector may be assumed to correspond to the horizontal and vertical coordinate directions without additional transformation. The applied force is prescribed to act on the body at an axial distance d_F from the projectile c.g. The sign of d_F is positive for a case in which the force is applied forward of the c.g., for example, near the nosetip. The relationship between the applied force and moment is prescribed as

$$\tilde{M}_1 = \tilde{F}_1 d_F \tag{15}$$

By substitution into the expressions already introduced, the relationship between the applied force and moment impulses is found to be

$$\tilde{\mathcal{M}}_1^* = \tilde{\mathcal{F}}_1^* d_F / d \tag{16}$$

The assumed relationship between the applied force and moment is convenient to satisfy the needs of the current work. More accurate (and more complex) expressions to define the applied force and moment disturbances can be used to refine the development of the approach for specific applications. For example, the expressions employed here, both in the analytical and numerical approaches, do not model the jet–body interactions.

Angular Motion with Singular Disturbance

The complex yaw angle $\tilde{\xi}$ is defined relative to the flight path (not relative to an Earth-fixed frame), consistent with the work of McCoy,[10] that is, $\tilde{\xi} = \alpha + i\beta$. The pitch angle α is positive for nose up and the yaw angle β is positive for nose right looking from the rear of the projectile. The projectile is assumed to be symmetric, nonspinning, statically stable, and in a relatively flat-fire trajectory. The projectile is further assumed to have no rocket thrust. Pitch damping, although important for certain applications, is presently neglected to focus attention on the methodology.

Under these assumptions, the linearized free-flight equation of angular motion with the inclusion of an applied force and moment can be derived by following the step-by-step procedure as given by McCoy[10] for the original equation with no applied impulses. The resulting equation of angular motion is

$$\tilde{\xi}'' - M\tilde{\xi} = \tilde{C}_{M1}^* / k_t^2 - \left(\tilde{C}_{N1}^*\right)' \tag{17}$$

in which the superscript prime denotes differentiation with respect to the flight path s. The nondimensional radius of gyration is $k_t = \sqrt{[I_t/(md^2)]}$ and $M = C_{M\alpha}^*/k_t^2$, in which $C_{M\alpha}^*$ is $C_{M\alpha}$ multiplied by the density factor. The term $(\tilde{C}_{N1}^*)'$ arises because the complex angle of attack is defined relative to the velocity vector rather than an Earth-fixed vector. The influence of this term can be visualized when a force disturbance is applied at the c.g. of a projectile having no angular motion, thus inducing nonzero angular motion.

If the applied force and moment disturbances are modeled as singular, then the equation of angular motion can be written as

$$\tilde{\xi}'' - M\tilde{\xi} = \tilde{\mathcal{J}}_1^* \delta(s - s_1) - \tilde{\mathcal{F}}_1^* \delta'(s - s_1) \tag{18}$$

in which $\tilde{\mathcal{J}}_1^* = \tilde{\mathcal{M}}_1^*/k_t^2$ and the Dirac delta function,[12] $\delta(s - s_1)$, is used. The solution in the nth interval (here, n is either 0 or 1) can be written in a form analogous to the free-flight cases given by Murphy[9] and McCoy,[10] referred to here as modal form:

$$\tilde{\xi} = K_{1,n} \exp(i\phi_{1,n}) \exp[i\phi'_{1,n}(s - s_0)] + K_{2,n} \exp(i\phi_{2,n}) \exp[i\phi'_{2,n}(s - s_0)] \tag{19}$$

in which the modal parameters are defined as follows: $K_{j,n}$ is the magnitude of jth epicyclic modal arm (here, j is either 1 or 2) for the nth interval, real and positive; $\phi_{j,n}$ is the reference phase angle of jth epicyclic modal arm for the nth interval, evaluated at $s = s_0$ and real; and $\phi'_{j,n}$ is the turning rate of jth epicyclic modal arm for the nth interval and real. For zero spin, as is the case here, the turning rates are related by $\phi' = \phi'_{1,n} = -\phi'_{2,n} = -M$.

The modal form of the solution is a parametric equation for an ellipse representing the modeled motion and is illustrated in Fig. 3. McCoy[10] refers to this type of motion as epicyclic, presumably in reference to the two terms on the right-hand side of the modal equation representing two modal arms, or rotating vectors, in the α, β complex plane. For one full cycle of motion, the summation of the two vectors etches the image of an ellipse in the complex plane. The eccentricity of the ellipse is determined by the relative magnitudes and phases of the two modal arms.

The solution to the equation of angular motion yields the following two conditions at s_1 for the complex angle of attack and its rate:

$$\tilde{\xi}\left(s_1^+\right) = \tilde{\xi}\left(s_1^-\right) - \tilde{\mathcal{F}}_1^* \tag{20}$$

$$\tilde{\xi}'\left(s_1^+\right) = \tilde{\xi}'\left(s_1^-\right) + \tilde{\mathcal{J}}_1^* \tag{21}$$

Following the same procedure as Cooper and Fansler,[2] the reference complex modal arms of the nth interval are defined as

$$\tilde{\mathcal{K}}_{1,n} = K_{1,n} \exp(i\phi_{1,n}) \tag{22}$$

$$\tilde{\mathcal{K}}_{2,n} = K_{2,n} \exp(i\phi_{2,n}) \tag{23}$$

The reference complex modal arms in the two adjacent intervals are related by

$$\tilde{\mathcal{K}}_{1,1} = \tilde{\mathcal{K}}_{1,0} - \tfrac{1}{2}\left[i\tilde{\mathcal{J}}_1^*/\phi' + \tilde{\mathcal{F}}_1^*\right] \exp[-i\phi'(s_1 - s_0)] \tag{24}$$

$$\tilde{\mathcal{K}}_{2,1} = \tilde{\mathcal{K}}_{2,0} + \tfrac{1}{2}\left[i\tilde{\mathcal{J}}_1^*/\phi' - \tilde{\mathcal{F}}_1^*\right] \exp[i\phi'(s_1 - s_0)] \tag{25}$$

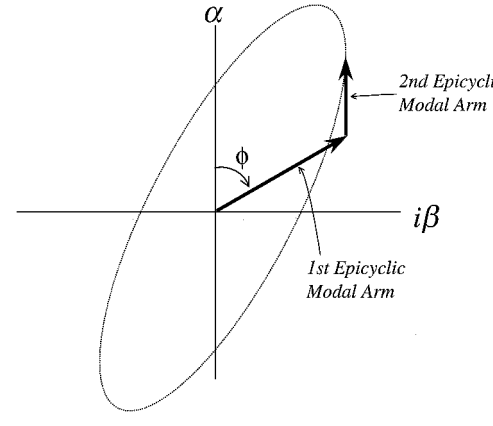

Fig. 3 Illustration of zero-damping epicyclic motion for nonspinning, fin-stabilized projectile.

The relative contributions to the angular motion from the applied translational and angular impulses can be ascertained by comparing the magnitudes of the terms $(\tilde{\mathcal{J}}_1^*/\phi')$ and $\tilde{\mathcal{F}}_1^*$. For the idealized projectile and lateral jet configuration to be presented subsequently, the contribution from the angular disturbance is found to be approximately 80 times greater than the contribution from the translational impulse. Therefore, it is prudent in the present work to ignore the applied translational impulse contribution to the angular motion and retain only the applied angular impulse contribution. The applied translational impulse can be as important as the applied angular impulse for cases in which the lateral jet is located closer to the projectile c.g. and/or the magnitude of the translational impulse is larger than in the present illustrative case.

In the present work, the applied angular impulse is written in complex polar form as follows:

$$\tilde{\mathcal{J}}_1^* = \mathcal{J}_1^* \exp(i\phi_1) \tag{26}$$

$$\mathcal{J}_1^* = \left|\tilde{\mathcal{J}}_1^*\right| \operatorname{sign}(d_F) \tag{27}$$

in which the orientation of the angular impulse is ϕ_1, as already defined. The scalar constant $\mathcal{J}_1^*$, which can be positive or negative, represents both the magnitude and sign of the angular impulse within the specified orientation. The term sign d_F equals 1 for $d_F \geq 0$ and -1 for $d_F < 0$. The relationship between the modal arms in adjacent intervals is then

$$K_{1,1}^2 = K_{1,0}^2 + \mathcal{J}_1^{*^2}/4\phi'^2 - \left(K_{1,0}\mathcal{J}_1^*/\phi'\right)\sin\Phi_{1,1} \tag{28}$$

$$K_{2,1}^2 = K_{2,0}^2 + \mathcal{J}_1^{*^2}/4\phi'^2 + \left(K_{2,0}\mathcal{J}_1^*/\phi'\right)\sin\Phi_{2,1} \tag{29}$$

in which

$$\Phi_{1,1} = \phi_{1,0} + (s_1 - s_0)\phi' - \phi_1 \tag{30}$$

$$\Phi_{2,1} = \phi_{2,0} - (s_1 - s_0)\phi' - \phi_1 \tag{31}$$

The phase shifts of the reference modal arms are then given by

$$\phi_{1,1} - \phi_{1,0} = \tan^{-1}\frac{\mathcal{J}_1^*\cos\Phi_{1,1}}{\mathcal{J}_1^*\sin\Phi_{1,1} - 2\phi' K_{1,0}} \tag{32}$$

$$\phi_{2,1} - \phi_{2,0} = \tan^{-1}\frac{\mathcal{J}_1^*\cos\Phi_{2,1}}{\mathcal{J}_1^*\sin\Phi_{2,1} + 2\phi' K_{2,0}} \tag{33}$$

Translational Motion with Singular Disturbance

The translational motion, also called swerve, is the motion of the projectile c.g. Following McCoy,[10] the free-flight swerve equation with no applied in-flight impulse can be written in complex notation as

$$y'' + iz'' = C_{L\alpha}^*\tilde{\xi} - g \tag{34}$$

in which y and z (not related to the $\bar{y}$ and $\bar{z}$ unit vectors mentioned earlier) are defined as

$$y = Y/d \tag{35}$$

$$z = Z/d \tag{36}$$

The left-hand side is the lateral acceleration of the projectile c.g. The right-hand side is the sum of aerodynamic and gravitational forces divided by the projectile mass.

The equation can be modified to include the applied in-flight force and moment impulses, giving

$$y'' + iz'' = C_{L\alpha}^*\tilde{\xi} + \tilde{C}_{N1}^* - g \tag{37}$$

The right-hand side now contains the applied translational disturbance $\tilde{C}_{N1}^*$. Also, the functional form of the complex angle of attack on the right-hand side now contains the additional terms representing the angular effects of the applied impulses. For the singular impulse model, the equation can be written as

$$y'' + iz'' = C_{L\alpha}^*\tilde{\xi} + \tilde{\mathcal{F}}_1^*\delta(s - s_1) - g \tag{38}$$

The solution to this differential equation can be written as

$$\tilde{r} = \tilde{r}_0 + \tilde{r}_0'(s - s_0) + \tilde{r}_T + \tilde{r}_L \tag{39}$$

The lateral displacement of the projectile c.g. is denoted here as $\tilde{r}$ and written in complex notation as

$$\tilde{r} = (y - y_g) + iz \tag{40}$$

in which the gravity drop y_g is removed from further consideration. The gravity drop is discussed by both Murphy[9] and McCoy[10] and remains unchanged from the free-flight case and is considered known. Before the individual terms that comprise the lateral displacement are addressed, note that the angular deviation, or jump, of the projectile from the pretrigger line of fire is traditionally related to the lateral deviation by

$$\tilde{\theta} = \tilde{r}/(s - s_0) \tag{41}$$

The first two terms describing the projectile lateral motion, $\tilde{r}_0$ and $\tilde{r}_0'(s - s_0)$, are initial conditions evaluated at $s = s_0$. The term $\tilde{r}_0$ is the projectile c.g. lateral location at s_0 and is typically taken to be zero, that is, the origin of the range coordinate system. The term $\tilde{r}_0'(s - s_0)$ is the lateral displacement of the projectile attributable to its lateral velocity at s_0, and this term's contribution to the lateral displacement is proportional to range, that is, a constant angular deviation.

The third term is the nonaerodynamic component of the lateral displacement attributable to the translational impulse and is denoted $\tilde{r}_T$. For the singular impulse model, the term can be written as follows, with r_1 and r_2 being dummy variables:

$$\tilde{r}_T = \int_{s_0}^{s}\int_{s_0}^{r_2}\tilde{\mathcal{F}}_1^*\delta(s - s_1)\,\mathrm{d}r_1\,\mathrm{d}r_2 \tag{42}$$

The term can be evaluated in the first interval as

$$\tilde{r}_T = (s - s_1)\tilde{\mathcal{F}}_1^* \tag{43}$$

Because the angular data can often be obtained more accurately in testing than the translational data, a useful alternate expression for $\tilde{r}_T$ is obtained by substituting the relationship between the applied translational and angular impulses, giving, in the first interval,

$$\tilde{r}_T = (s - s_1)\tilde{\mathcal{J}}_1^* k_t^2 d/d_F \tag{44}$$

This term's contribution to the projectile angular deviation at range $(s - s_0)$ is denoted here as $\tilde{\theta}_T$ and is given in radians as

$$\tilde{\theta}_T = \frac{\tilde{r}_T}{(s - s_0)} = \frac{(s - s_1)}{(s - s_0)}\frac{\tilde{\mathcal{J}}_1^* k_t^2 d}{d_F} \tag{45}$$

The fourth term, denoted $\tilde{r}_L$, is the lateral displacement attributable to all aerodynamic lift effects, that is,

$$\tilde{r}_L = C_{L\alpha}^*\int_{s_0}^{s}\int_{s_0}^{r_2}\tilde{\xi}\,\mathrm{d}r_1\,\mathrm{d}r_2 \tag{46}$$

The lift terms, on carrying out the double integration, can be separated into the sum of two specific complex terms, that is,

$$\tilde{r}_L = \tilde{r}_E + \tilde{r}_A \tag{47}$$

The epicyclic component of the swerve $\tilde{r}_E$ can be algebraically simplified and expressed in terms of the motion parameters and aerodynamic coefficients in the first interval as

$$\tilde{r}_E = k_t^2(C_{L\alpha}/C_{M\alpha})\left(\tilde{\xi} - \tilde{\xi}_0 - \tilde{\mathcal{F}}_1^*\right) \tag{48}$$

The epicyclic component of the swerve is the only component that fluctuates with respect to range. The magnitude of the epicyclic component for the idealized projectile with small yaws of the current study, however, remains on the order of the projectile diameter. For

the large ranges being considered here, the epicyclic component is not a significant contributor to lateral displacement, except in terms of validating the analytical approach.

The remaining aerodynamic lift terms can be collected and simplified in the first interval as

$$\tilde{r}_A = -k_t^2(C_{L\alpha}/C_{M\alpha})\left[(s-s_0)\tilde{\xi}_0' + (s-s_1)\tilde{\mathcal{J}}_1^*\right] \tag{49}$$

This term's contribution to the projectile angular deviation at range $(s-s_0)$ is denoted here as $\tilde{\theta}_A$ and is

$$\tilde{\theta}_A = \frac{\tilde{r}_A}{(s-s_0)} = -k_t^2\frac{C_{L\alpha}}{C_{M\alpha}}\left[\tilde{\xi}_0' + \frac{(s-s_1)}{(s-s_0)}\tilde{\mathcal{J}}_1^*\right] \tag{50}$$

In Eq. (50), the contribution from the initial projectile angular rate $\tilde{\xi}_0'$ is recognizable as the aerodynamic jump as expressed by Murphy[9] and McCoy[10] for a nonspinning, statically stable projectile. The expression demonstrates the equivalency that exists between the angular impulse imparted to the projectile by the gun and the angular impulse imparted by the applied in-flight angular impulse. If the applied angular impulse occurs close to the muzzle in comparison to the target range, the expression can be approximated as

$$\tilde{\theta}_A = -k_t^2(C_{L\alpha}/C_{M\alpha})\left(\tilde{\xi}_0' + \tilde{\mathcal{J}}_1^*\right) \tag{51}$$

Angular Motion with Finite Pulse Disturbance

If the applied lateral translational and angular disturbances are modeled as finite pulse disturbances with nonzero duration, as described earlier, then the equation of angular motion can be written as

$$\tilde{\xi}'' - M\tilde{\xi} = \tilde{\mathcal{J}}_1^*[h(s-s_1+\Delta s_1) - h(s-s_1)] - \tilde{\mathcal{F}}_1^*[h'(s-s_1+\Delta s_1) - h'(s-s_1)] \tag{52}$$

The general solution, with the simplification that $\phi' = \phi'_{1,n} = -\phi'_{2,n}$ is

$$\begin{aligned}\tilde{\xi} &= K_{1,0}\exp(i\phi_{1,0})\exp[i\phi'(s-s_0)] \\ &\quad + K_{2,0}\exp(i\phi_{2,0})\exp[-i\phi'(s-s_0)] \\ &\quad - \tilde{\mathcal{J}}_1^*/(2\phi'^2)\{h(s-s_1+\Delta s_1)\{\exp[i\phi'(s-s_1+\Delta s_1)] \\ &\quad + \exp[-i\phi'(s-s_1+\Delta s_1)] - 2\} - h(s-s_1)\{\exp[i\phi'(s-s_1)] \\ &\quad + \exp[-i\phi'(s-s_1)] - 2\}\} + i\tilde{\mathcal{F}}_1^*/(2\phi'^2)\{h(s-s_1+\Delta s_1) \\ &\quad \times \{\exp[i\phi'(s-s_1+\Delta s_1)] - \exp[-i\phi'(s-s_1+\Delta s_1)]\} \\ &\quad - h(s-s_1)\{\exp[i\phi'(s-s_1)] - \exp[-i\phi'(s-s_1)]\}\}\end{aligned} \tag{53}$$

The solution in the nth interval can be written in modal form as

$$\begin{aligned}\tilde{\xi} &= K_{1,n}\exp(i\phi_{1,n})\exp[i\phi'(s-s_0)] \\ &\quad + K_{2,n}\exp(i\phi_{2,n})\exp[-i\phi'(s-s_0)]\end{aligned} \tag{54}$$

although this particular form does not apply within the subinterval itself. Whereas the modal form for the finite pulse model is the same as for the singular disturbance model, the values of the modal parameters themselves (with the exception of ϕ') are different. The expressions relating the modal parameters of adjacent intervals, however, are not needed to solve the swerve equation for the finite pulse model and are not included here. It will be shown that, for the conditions of interest here, the finite pulse model gives only slightly modified expressions as the singular disturbance model for the projectile lateral motion.

Translational Motion with Finite Pulse Disturbance

The swerve equation for the finite pulse model can be written as

$$y'' + iz'' = C_{L\alpha}^*\tilde{\xi} + \left(\tilde{\mathcal{F}}_1^*/\Delta s_1\right)[h(s-s_1+\Delta s_1) - h(s-s_1)] - g \tag{55}$$

The functional form of the complex angle of attack $\tilde{\xi}$ on the right-hand side contains the additional terms representing the effects of the finite pulse disturbance on the angular motion, as already presented. The solution can be written in the same form as for the singular disturbance model, that is,

$$\tilde{r} = \tilde{r}_0 + \tilde{r}_0'(s-s_0) + \tilde{r}_T + \tilde{r}_L \tag{56}$$

The terms $\tilde{r}_0$ and $\tilde{r}_0'(s-s_0)$ are unchanged from the singular disturbance model. The nonaerodynamic component of the lateral displacement attributable to the translational impulse is now

$$\tilde{r}_T = \int_{s_0}^{s}\int_{s_0}^{r_2}\frac{\tilde{\mathcal{F}}_1^*}{\Delta s_1}[h(s-s_1+\Delta s_1) - h(s-s_1)]\,\mathrm{d}r_1\,\mathrm{d}r_2 \tag{57}$$

and is evaluated in the first interval as

$$\tilde{r}_T = (s-s_1)\tilde{\mathcal{F}}_1^* + \tfrac{1}{2}\Delta s_1\tilde{\mathcal{F}}_1^* \tag{58}$$

The first term on the right-hand side of Eq. (58) is identical to that of the singular disturbance case. The second term is the difference between the finite pulse and singular disturbance models for this component of the swerve and is denoted $\Delta\tilde{r}_T$ and given as

$$\Delta\tilde{r}_T = \tfrac{1}{2}\Delta s_1\tilde{\mathcal{F}}_1^* \tag{59}$$

As in the singular disturbance case, the lateral displacement attributable to aerodynamic lift $\tilde{r}_T$ can be separated into components $\tilde{r}_E$ and $\tilde{r}_A$. The epicyclic swerve component $\tilde{r}_E$ for the finite pulse disturbance model differs slightly from that of the singular disturbance model. However, like the singular disturbance model, the magnitude of $\tilde{r}_E$ is still small and is still not considered to be a significant contributor to the projectile angular deviation under the current conditions.

The remaining lift terms can be collected and simplified to express $\tilde{r}_A$ in the first interval as

$$\tilde{r}_A = -k_t^2(C_{L\alpha}/C_{M\alpha})\left[(s-s_0)\tilde{\xi}_0' + (s-s_1)\tilde{\mathcal{J}}_1^* + \tfrac{1}{2}\Delta s_1\tilde{\mathcal{J}}_1^*\right] \tag{60}$$

which is the same as for the singular disturbance model but with an additional term representing the difference between the finite pulse and singular disturbance models for this component of the swerve. The difference is denoted $\Delta\tilde{r}_A$ and given as

$$\Delta\tilde{r}_A = -\tfrac{1}{2}k_t^2(C_{L\alpha}/C_{M\alpha})\Delta s_1\tilde{\mathcal{J}}_1^* \tag{61}$$

Results

Idealized Finned Projectile

An idealized 120-mm finned projectile geometry is adopted to compare the analytical results with those from a numerical trajectory simulation code. Figure 4 shows the idealized projectile geometry and Table 1 lists the defining parameters. The configuration is typical of the current class of 120-mm armor-piercing, fin-stabilized, discarding sabot kinetic energy ammunition launched from the Abrams M1A1 tank.

The aerodynamic pitch-plane center of pressure is determined from the prescribed values of pitching moment coefficient $C_{M\alpha}$ and normal force coefficient $C_{L\alpha}$. Both coefficients are held constant at

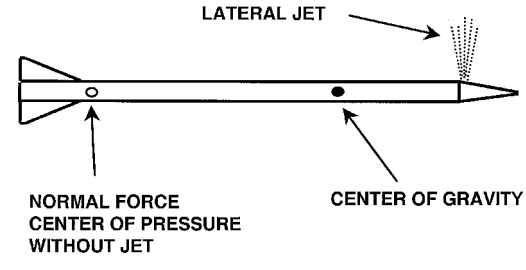

Fig. 4 Idealized finned projectile and lateral pulse generator.

Table 1 Idealized projectile and lateral pulse generator properties

Property	Value
Rod diameter d	0.0254 m
Mass m	5.0 kg
Length	0.8 m
Location of c.g. from base	0.5 m
Transverse moment of inertia I_t	0.2 kg · m^2
Pitching moment coefficient $C_{M\alpha}$	−100 caliber/rad
Lift force coefficient $C_{L\alpha}$	10/rad
Location of lateral jet relative to c.g. d_F	0.2 m

Table 2 Finite pulse disturbances for cases 2 and 3

Pulse parameter	Case 2	Case 3
Force magnitude, N	100	100
Force orientation ϕ_1, deg	180	90
Range where impulse begins, m	984	984
Range where impulse ends, m	1000	1000
Duration, ms	10	10
Translational impulse, N · s	1	1

their launch values, as is the total velocity. The projectile is prescribed to have a lateral impulse jet situated at an axial location that would correspond to a location near the nose. As shown in Table 2, the lateral impulse jet has a total impulse of 1 N · s (equivalent to a 100-N force with a 10-ms duration), typical of an off-the-shelf component.

Case 1: No Impulse

The numerical trajectory simulation code written by Costello[11] was used to generate trajectories to compare to the analytical results. The numerical code uses a fourth-order Runge–Kutta method to integrate the equations of motion, limited to six degrees of freedom in the present study. To produce consistency in the comparisons, two aerodynamic conditions were enforced through the aerodynamic inputs to the numerical code. First, the drag coefficient was specified to be zero. Second, the relationship between the pitch-damping coefficient C_{Mq} and the lift coefficient $C_{L\alpha}$ was specified to be

$$C_{Mq} = k_t^2 C_{L\alpha} \tag{62}$$

These two conditions produce the zero-damping condition implicit in the analytical equation of angular motion by allowing the coefficient of the $\tilde{\xi}'$ term to be zero. The relationships are easily recognized in the discussions by both Murphy[9] and McCoy.[10]

Many different cases with varying launch conditions and in-flight lateral impulses were examined during the course of the study, but the discussion here is limited to three illustrative cases, as summarized in Tables 2 and 3. For all three cases to be presented, the launch velocity is prescribed to be 1600 m/s (approximately Mach 4.7). The gun elevation is prescribed to be zero, that is, horizontal to the ground. The projectile is prescribed to exit the gun with no lateral translational rate relative to the pretrigger line of fire, that is, the components of $\tilde{r}_0'$ are zero in both azimuth and elevation. The pitch and yaw angles are prescribed to be zero at launch. The projectile is nonspinning.

In case 1, no in-flight lateral impulse is applied. Although the existing theory of epicyclic motion as described by Murphy[9] and McCoy[10] is adequate to model this case, some defining characteristics of the projectile motion can be ascertained for comparison to the subsequent cases. The initial angular rate is prescribed to be 5 rad/s, with the nose rotating directly upward. The angular motion is planar and sinusoidal, occurring strictly in the vertical ($\beta = 0$) plane. Figure 5 shows the numerical and analytical results for pitch angle vs range from launch to 1-km range. The maximum pitch angle is approximately 2.9 deg. Because no damping is used in either the analytical or numerical models, the amplitude of the sinusoidal motion remains constant throughout the flight.

Figure 6 shows the lateral displacement vs range from the numerical and analytical methods for case 1 from launch to 3-km range. Like the angular motion, the translational motion is planar,

Table 3 Launch conditions

Condition	Value
V_0	1600 m/s
α_0	0 deg
β_0	0 deg
$(d\alpha/dt)_0$	0.5 rad/s
$(d\beta/dt)_0$	0 rad/s
$(dy/dt)_0$	0 m/s
$(dz/dt)_0$	0 m/s

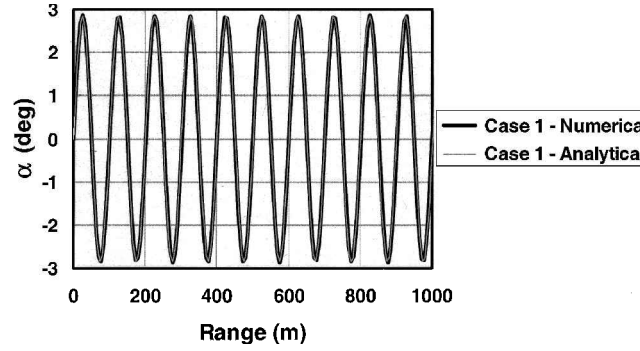

Fig. 5 Pitch angle vs range, case 1.

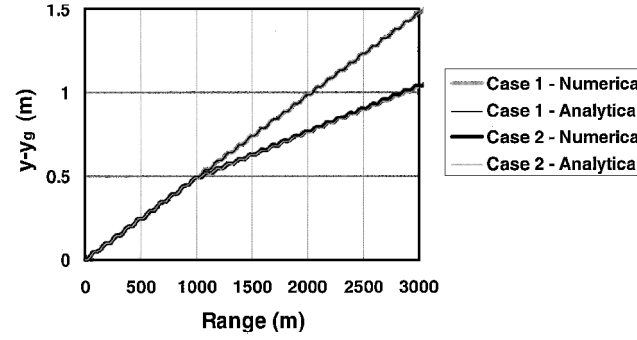

Fig. 6 Vertical displacement vs range, cases 1 and 2.

occurring strictly in the vertical ($z = 0$) plane. The numerical and analytical results for case 1 are indistinguishable in Fig. 6. The vertical displacement from the two approaches is approximately 1.478 m upward at 3-km range and the numerical and analytical approaches differ by less than 1 mm. The fluctuating component of the swerve is seen to be small (on the order of a few centimeters) compared to the total swerve, indicating that a good estimate of lateral displacement can be obtained for large ranges even if the fluctuating component is ignored. For short-range applications, as is common in testing scenarios, the fluctuating component could be important.

Case 2: In-Plane Impulse

Case 2 is the same as case 1, except that the lateral jet is engaged at some location in midflight. The orientation of the jet relative to the ground is such that the jet releases upward, resulting in a downward force applied to the projectile nose (that is, $\phi_1 = 180$ deg). The vertical impulse is, therefore, applied within the vertical plane of motion to which the projectile is already adhering. In the numerical case, the jet force is modeled as a finite pulse disturbance initiated at 0.615 s into the flight (corresponding to 984-m range) with a duration of 10 ms, that is, occurring over a range of approximately 16 m. Two analytical solutions were generated, the first using a singular disturbance occurring at 992-m range, and the second using a finite pulse disturbance as given in Table 2.

The vertical displacement obtained from the numerical approach and the analytical approach having the singular disturbance is included in Fig. 6, along with the result from case 1. The vertical displacement is calculated using the analytical approach to be 1.029 m at 3-km range, almost 0.5 m below that of case 1. The analytical and numerical results are indistinguishable in Fig. 6. The

numerical results, as expected, were found to be sensitive to the prescribed fixed time-step size because the Runge–Kutta integration scheme must numerically capture the applied force and moment discontinuities at t_1 and $t - \Delta t_1$. A numerical time step of 0.25 ms yielded a vertical displacement that differed from the analytical calculation having a singular disturbance by approximately 1 cm at 3-km range. When the numerical time step size is decreased to 0.025 ms, the difference of vertical displacement between the numerical and analytical approaches was reduced to approximately 1 mm at 3-km range.

The analytical result generated using the finite pulse model were virtually unchanged from the singular disturbance model. The difference in the nonaerodynamic lateral displacement component $\Delta\tilde{r}_T$ was calculated to be approximately 1 mm at 3-km range. The difference in the aerodynamic component $\Delta\tilde{r}_A$ was calculated to be approximately 0.13 mm. Both of these differences are independent of range. It is concluded that, for case 2, the difference between the lateral displacement calculated by the singular impulse model and the square impulse model is insignificant for this case. A substantial increase in either the impulse magnitude or the impulse duration would be required before the differences between the singular impulse model and the square impulse model become significant.

The analytical result of case 2 shows that the applied impulse causes a lateral course correction of 0.437 m downward from the uncorrected flight of case 1. The translational, that is, nonaerodynamic component provides 56% of the lateral course correction, whereas the angular, that is, aerodynamic, component provides the remaining 44%, illustrating the importance of including aerodynamic effects when considering the effect of lateral impulses.

Figure 7 shows the pitch angle as a function of range for cases 1 and 2 as obtained from the analytical and numerical approaches. Figure 7 shows the detailed behavior of the pitch angle at and near the range at which the lateral jet impulse is applied. Although no strict quantitative characterization is made between the analytical and numerical results, both the amplitude and phase of the sinusoidal motions appear qualitatively correct to within the scale of the Fig. 7. The application of the jet impulse produces a slight shift in phase as well as a decrease of maximum pitch angle of approximately 0.5 deg.

In general, the change in maximum angle of attack produced by the lateral jet can be positive or negative depending on where in the yaw cycle the impulse is applied. The analytical approach has the ability to characterize the pitching and yawing behavior in closed form in this manner, although no further discussion is made of this aspect at this time. Note that a more advanced application of the analytical approach is the simultaneous control of lateral displacement and angular behavior. Such an approach leads to the design of guidance maneuvers that not only improve accuracy but also reduce the in-flight maximum angle of attack.

Case 3: Out-of-Plane Impulse

Case 3 is the same as case 2 except that the orientation of the jet is such that the jet releases to the gunner's left, resulting in the projectile nose being forced to the gunner's right, that is, $\phi_1 = 90$ deg. This is a horizontal impulse is applied out of the plane of the existing vertical motion. The resulting angular and translational motions are

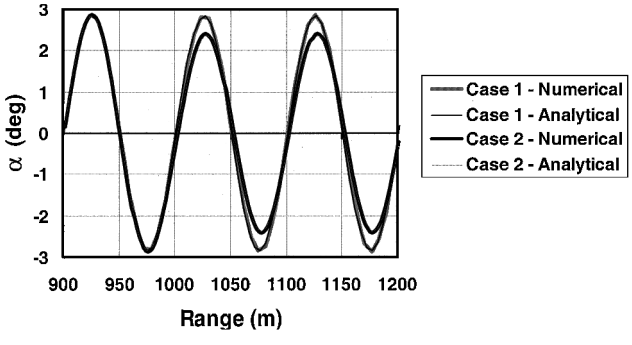

Fig. 7 Pitch angle vs range, cases 1 and 2.

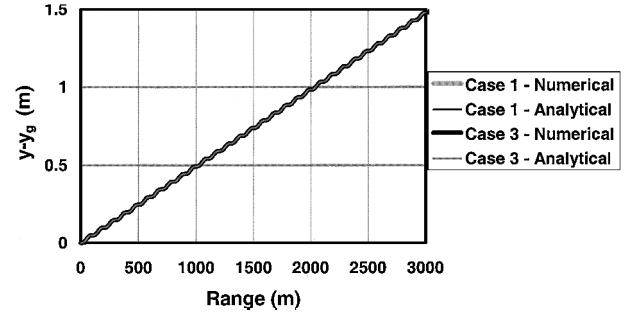

Fig. 8 Vertical displacement vs range, cases 1 and 3.

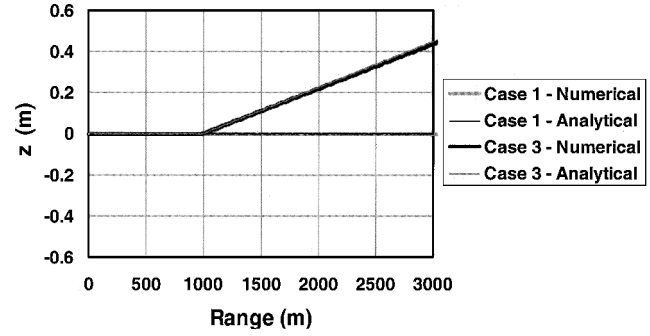

Fig. 9 Horizontal displacement vs range, cases 1 and 3.

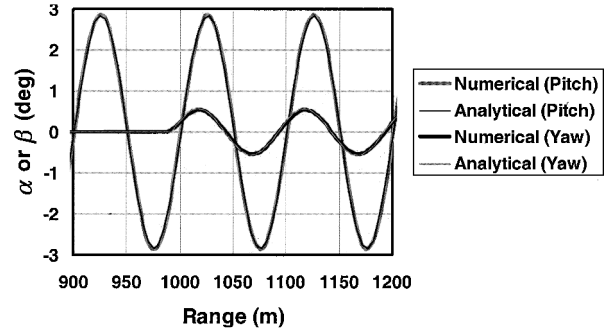

Fig. 10 Pitch and yaw angles vs range, case 3.

no longer limited to the vertical plane. Figure 8 shows the analytical and numerical results of the vertical displacement for case 3. The results are plotted with those from case 1, and all four lines are indistinguishable, demonstrating that the vertical translational motion is decoupled from the horizontal impulsive disturbance.

Figure 9 shows the analytical and numerical results of horizontal displacement for case 3, along with the results from case 1. Up-range from the range at which the jet is initiated, the horizontal displacement is zero for both cases. However, for case 3, the impulse produces a horizontal displacement to the gunner's right, whereas the horizontal displacement for case 1 remains zero throughout the flight. The horizontal displacement for case 3 is equal in magnitude to the vertical course correction observed in case 2. Also, as in case 2, the difference between the analytical and numerical result is approximately 1 cm at 3-km range and is attributable to a numerical integration error that is affected by the time-step size.

Finally, Fig. 10 shows the analytical and numerical results of the angular motion for case 3. As in Fig. 9, Fig. 10 shows the detailed behavior near the range at which the lateral jet impulse is applied. The pitching motion is unaffected by the lateral jet; however, the yawing motion is affected. Up-range of the range at which the lateral jet is applied, the yaw angle is equal to zero. The impulse produces yawing motion that reaches a maximum value greater than 0.5 deg. The analytical and numerical results qualitatively compare to within the scale of Fig. 10, and differences are quantitatively similar to those of case 2.

Conclusions

An analytical approach for quantifying the effect of a simple in-flight impulsive disturbance acting on a nonspinning finned projectile has been presented. The approach is based on the incorporation of a specific class of modeled applied lateral translational and angular impulsive disturbances into the equations of projectile free-flight motion. The modified equations were solved to obtain the angular and translational motion of the projectile, and the components of the translational motion were extracted.

A sample of results from the analytical model was compared to results obtained from an existing numerical trajectory simulation code. The lateral impulse simulated a constant magnitude, constant direction, 1 N · s lateral jet impulse (100 N with a duration of 10 ms) located on the nose of the projectile and initiated at a range of 1 km. The calculated lateral displacement of the projectile, as well as the components of the displacement, consistently agreed with the numerical results to approximately 1 mm at 3-km range. The results showed that the lateral jet force and moment disturbances produced a lateral displacement of almost 0.5 m at 3-km range. The epicyclic swerve component was found to be on the order of a few centimeters, indicating that its importance was minimal for long-range applications but possibly significant for short-range applications.

Two different analytical models for the applied disturbances were presented: a singular disturbance model and a finite pulse disturbance model. For the impulse magnitude and duration of the prescribed jet, insignificant differences were found between the two models. It was concluded that a substantial increase in the magnitude and/or duration of the square wave impulse would be necessary before the difference in lateral displacement obtained using the square wave and singular impulse models would be significant.

The analytical model provides useful closed-form analytical solutions to the equations of angular and translational motion for a projectile acted on by this specific class of generalized impulsive disturbances. Although the lengthy mathematics of the derivation and solution procedures have been omitted here for brevity, the final expressions are found to be simple and straightforward. The simplicity of the expressions suggests that reduced computational overhead for onboard course correction instrumentation may be obtained. Furthermore, the approach has an application in the testing and development of smart munitions, providing a framework for analyzing and predicting free-flight motion of a projectile undergoing applied course correction maneuvers.

The impulse model was presented here for nonspinning, statically stable projectiles, neglecting pitch damping. Typically, finned projectiles are adequately damped and have low spin rates. The generalization to include damping and spin is a straightforward extension of the current approach. In addition, the complete incorporation of the translational impulse into the angular equations is desirable to accommodate certain classes of larger impulsive disturbances. The methodology is easily extended to include successive disturbances to facilitate the modeling of highly complex motions and course correction maneuvers.

References

[1]McCoy, R. L., "The Effect of Yaw Cards on the Pitching and Yawing Motion of Symmetric Projectiles," U.S. Army Ballistic Research Lab., Rept. BRL-TR-3338, Aberdeen Proving Ground, MD, May 1992.

[2]Cooper, G., and Fansler, K., "Yaw Card Perturbation of Projectile Dynamics," U.S. Army Research Lab., Rept. ARL-TR-1258, Aberdeen Proving Ground, MD, Jan. 1997.

[3]Plostins, P., "A Method for Extracting the Sabot Discard Impulse from Transitional Ballistic Data," U.S. Army Research Lab., Rept. BRL-TR-3244, Aberdeen Proving Ground, MD, June 1991.

[4]Iosilevskii, G., and Farber, N., "Effect of a Spherical Explosion Upon the Flight Path and Spatial Orientation of a Projectile," *International Journal of Impact Engineering*, Vol. 25, No. 2, 2001, pp. 187–191.

[5]Yalamanchili, R. J., and D'Amico, W. P., "Feasibility Study of an Active Damping Concept as Applied to a 2.75-inch Rocket," U.S. Army Ballistic Research Lab., Rept. BRL-MR-3925, Aberdeen Proving Ground, MD, June 1991.

[6]Fowler, R., Gallop, J., Lock, C., and Richmond, H., "Aerodynamics of a Spinning Shell," *Philosophical Transactions of the Royal Society of London, Series A: Mathematical and Physical Sciences*, Vol. 221, 1920, pp. 295–387.

[7]McShane, E., Kelley, J., and Reno, F., *Exterior Ballistics*, 1st ed., Univ. of Denver Press, Denver, CO, 1953, pp. 600–641.

[8]Nicolaides, J., "On the Free Flight Motion of Missiles Having Slight Configurational Asymmetries," U.S. Army Ballistic Research Lab., Rept. 858, Aberdeen Proving Ground, MD, June 1953; also Inst. of Aeronautical Sciences Preprint 395, Jan. 1953.

[9]Murphy, C. H., "Free Flight Motion of Symmetric Missiles," U.S. Army Ballistic Research Lab., Rept. BRL-R-1216, Aberdeen Proving Ground, MD, July 1963.

[10]McCoy, R. L., *Modern Exterior Ballistics*, 1st ed., Schiffer, Atglen, PA, 1998, pp. 221–247.

[11]Costello, M. F., "Potential Field Artillery Projectile Improvement Using Movable Canards," U.S. Army Research Lab., Rept. ARL-TR-1344, Aberdeen Proving Ground, MD, April 1997.

[12]Lighthill, M. J., *Introduction to Fourier Analysis and Generalized Functions*, 1st ed., Cambridge Univ. Press, New York, 1958, pp. 10, 11, 30, and 31.

C. A. Kluever
Associate Editor